Available online at www.sciencedirect.com
ScienceDirect
Journal of Power Sources 165 (2007) 152–170
JOURNAL OF POWER SOURCES
www.elsevier.com/locate/jpowsour

Dynamic analysis and linear control strategies for proton exchange membrane fuel cell using a distributed parameter model

R.N. Methekar, V. Prasad *, R.D. Gudi

Department of Chemical Engineering, Indian Institute of Technology, Bombay, Powai, Mumbai 400076, Maharashtra, India

Received 30 August 2006; received in revised form 15 November 2006; accepted 17 November 2006
Available online 18 January 2007

Abstract

To satisfy high power density demand in proton exchange membrane fuel cells (PEMFCs), a robust control strategy is essential. A linear ratio control strategy is examined in this work. The manipulated variables are selected using steady-state relative gain array (RGA) analysis to be the inlet molar flow rates of hydrogen and coolant, and the controlled variables are average power density and average solid temperature, respectively. By selecting proper manipulated variables, the PEMFC does not exhibit sign change in gain and hence can be controlled by using a linear controller. Transfer function models obtained from step tests on the distributed parameter PEMFC model are used to design controllers for the multiple input–multiple output (MIMO) system. In addition, a ratio control strategy is proposed and evaluated, where the inlet molar flow rate of oxygen is used as a dependent manipulated variable and changed in a constant ratio with respect to the inlet molar flow rate of hydrogen. Simulation results show that the ratio control strategy provides a faster response than a MIMO control strategy. This ratio control strategy is able to circumvent the problem of oxygen starvation, and the increase in average solid temperature is small as compared to the MIMO control strategy.

Keywords: Identification; Linear control; Ratio control; PEMFC

1. Introduction

Fuel cells are devices that convert the chemical energy of reactants (fuel and oxidant) directly into electrical energy. Fuel cells offer various economic and environmental advantages over internal combustion engines and batteries. Due to these advantages, enormous interest has been created in fuel cell technology for terrestrial applications. Particularly, the proton exchange membrane fuel cell (PEMFC) [1] offers many advantages over other fuel cells; hence, this device has the potential to become the primary source for power in the coming era.

In the literature, a large number of steady-state models are available, which focus mainly on designing the PEMFC and choosing the fuel cell operating point. Baschuk and Xianguo [2] have developed a model considering all three reasons of polarization in a unified fundamental approach. This model incorporates all the essential fundamental physical and electrochemical processes occurring in the membrane electrolyte, cathode catalyst layer, electrode backing and flow channels. Also, they studied the effects of variable degree of water flooding in the cathode catalyst layer and/or the cathode electrolyte backing on the cell performance. They found that the PEMFC exhibits two different patterns of flooding, changing with pressure and temperature, using oxygen, but found only one pattern with air. They concluded that power density substantially reduces and heat produced increases with flooding. Voss et al. [3] suggested a technique for water removal from the PEMFC. The fundamental premise of the anode water removal technique was to modify the water concentration profile of the solid polymer electrolyte membrane fuel cell such that water at the cathode catalyst layer diffused through the membrane and was removed via the anode reactant gas stream. They also suggested that the primary effect of this method was the reduction in cathode overpotential without substantial reduction in membrane ionic conductivity. Nguyen and White [4] have developed a model to investigate the effectiveness of three humidification designs. They showed that at high current density (>1 A cm^{-2}), ohmic

Abbreviations: CSTR, continuous stirred tank reactor; IMC, internal model control; MIMO, multiple input multiple output; MPC, model predictive control; NIMC, nonlinear model predictive control; PEMFC, proton exchange membrane fuel cell; PID, proportional integral control

* Corresponding author. Tel.: +91 22 2576 7234; fax: +91 22 2572 6895.
E-mail address: prasad@che.iitb.ac.in (V. Prasad).

0378-7753/$ – see front matter © 2006 Elsevier B.V. All rights reserved.
doi:10.1016/j.jpowsour.2006.11.047

Nomenclature

a	water activity
A	heat exchange area per unit length (cm)
C_p	molar heat capacity (J (gmol K)$^{-1}$)
d	channel height (cm)
D^*	diffusion coefficient of water in membrane (cm^2 s^{-1})
e	membrane area per unit length (cm)
f	cross-section of solid (cm^2)
F	Faraday's constant (C equivalent^{-1})
h	channel length (cm)
ΔH	enthalpy of overall reaction (J mol^{-1})
ΔH_{vap}	enthalpy of water evaporation (J mol^{-1})
I	current density (A cm^{-2})
I_0	exchange current density (A cm^{-2})
k	heat conduction coefficient (W (cm K)$^{-1}$)
k_i	steady-state gain
k_c	condensation rate constant (s^{-1})
K_{cc}	controller gain
L	total length of channel (cm)
m	manipulated variable
M	molar flow rate (mol s^{-1})
n	number of electrons taking part in charge reactions
P	pressure (atm)
T	temperature (K)
U	convective heat transfer coefficient (W cm^{-2} K^{-1})
y_1	average power density (W cm^{-2})
y_2	average solid temperature (K)

Greek letters

α	ratio of water molecules per proton (molecules proton^{-1})
η	overpotential (V)
ρ	density (g cm^{-3})
$\rho_{m,dry}$	dry membrane density (g cm^{-3})
σ	surface tension (N cm^{-1})
τ	time constant (s)

Superscripts

l	liquid
sat	saturation
v	vapor

Subscripts

a	anode
avg	average
b	bulk
c	cathode
cool	coolant
D	derivative
H_2	hydrogen
inf	ambient
I	integral
oc	open circuit
O_2	oxygen
s	solid
w	water

losses in the membrane account for a large fraction of the voltage loss in the fuel cell and back-diffusion of water from the cathode side of membrane was insufficient to keep the membrane hydrated. Consequently, to minimize these problems, they suggested that the anode stream must be humidified when oxygen is used, whereas when air is used instead of pure oxygen, both the streams must be humidified. Fuller and Newman [5] simulated a PEMFC operation under the condition of moist gas in the electrodes. They obtained the water distribution in the membrane and the water flux across it. Bernardi and Verbrugge [6] formulated a simplified one-dimensional model for liquid water transport in porous electrodes assuming a constant liquid volume fraction and no interactions between liquid and gas flows. Wang et al. [7] studied gas–liquid two phase flow and transport in the air operated PEMFC as well as the direct methanol fuel cell. They found that water liquid and vapor transport was controlled by capillary action and molecular diffusion. At low current densities, the cathode activation overpotential was solely responsible for the potential losses at the cathode. At higher current densities, more oxygen was consumed and more water was generated at membrane/cathode interface due to electrochemical reactions and water transport across the membrane from the anode. These effects result in a slightly steeper slope of the cathode potential curve upon the threshold current density. Wohr et al. [8] subdivided the PEMFC into different components, i.e., gas distributor, gas diffusion layer and catalytic layer, and membrane. They stated that an increase in the temperature of the humidifier results in a higher humidity of the anodic gas flow which in turn increases the membrane conductivity and lowers the potential drop across the membrane. They also found that voltage drops when air was used instead of oxygen. They favored the use of cooling plates in the fuel cell stack to reduce the temperature of the cell. Most of the above models provide an understanding of the effects of liquid and vapor water transport on the performance of the PEMFC, in addition to the effect of using oxygen or air at the cathode.

However, most of these models are not suitable for control studies [9]. There are relatively fewer dynamic models proposed in the literature that have studied transient behavior [10,11] and control of fuel cells. Pukrushpan et al. [12] focused on three major control subsystems, viz. air/fuel supply, water management and heat management in fuel cell systems. Using feedback and feedforward control, they maintained an excess oxygen ratio and reported the net system power (after subtracting the extra power required for maintaining the excess oxygen ratio and overcoming parasitic losses from the output power) obtained from the fuel cell. Vahidi et al. [13] focused on the starvation problem in a hybrid system, where a fuel cell was coupled with a power source

that responded quickly through the use of an ultracapacitor. They used a model predictive control strategy to avoid starvation and simultaneously match an arbitrary level of current demand. Golbert and Lewin [14] showed that fuel cells exhibit a sign change in gain between power density and voltage, which precluded the use of a fixed gain controller; hence, they proposed the use of adaptive and model predictive controllers. They used current density and inlet coolant temperature as manipulated variables to control the power density. They also proposed a CSTRs-in-series based reduced order model for controller design, which neglected the spatial variations in the fuel cell. Golbert and Lewin [15] also achieved robust performance and improved fuel cell efficiency by using a model predictive control based strategy. Na et al. [16] used a lumped parameter model for the PEMFC. The nonlinear model was linearized by exact linearization, and the controller was designed based on the linear model and implemented on the nonlinear system, where voltage was controlled by manipulating both fuel and oxidant input flow rate and current. Lauzze and Chmielewski [17] controlled the power output from a fuel cell by using voltage as a manipulated variable cascaded with current density. They pointed out that at lower power density, the relative humidity increases and the voltage drops. To overcome this problem, relative humidity and/or temperature control was implemented by manipulating coolant jacket flow rate cascaded with cathode temperature. They also addressed the problem of oxygen starvation. A lumped parameter model based on mass and energy balances and the electrochemistry of the fuel cell system was used in their study. Yerramalla et al. [18] studied the dynamic response of fuel cell stack preserving the nonlinearities of the fuel cell including the effect of inverter load.

Most of the preceding work on PEMFC control neglected the effect of spatial variations while designing the controller; these spatial variations affect the dynamics of the fuel cell and need to be included while developing dynamic models for control purposes. Also, proper selection of the suitable manipulated variables for regulating the desired controlled outputs has received no attention in the literature.

In the present work, the distributed parameter model proposed by the Yi and Nguyen [19] and further extended by Golbert and Lewin [14] has been used to develop dynamic models and to analyze the control performance. This model is an along-the-channel model that takes spatial variations into consideration. Some peculiar and interesting dynamics resulting from the spatial structure are analyzed in this paper. Further, the PEMFC is considered as a multi input and multi output (MIMO) system where average power density and average solid temperature are the two controlled outputs. The transient behavior of the PEMFC has been studied for various manipulated variables such as the inlet molar flow rate of oxygen and hydrogen, the inlet gas temperature at the anode and the cathode, and the inlet molar flow rate of coolant. The steady-state relative gain array (RGA) analysis has been used to decide which manipulated variables are suitable for controlling the outputs, and it indicates that the inlet molar flow rate of hydrogen and coolant are the suitable manipulated variables for controlling average power density and average solid temperature, respectively. To account for disturbances in inlet coolant states (temperature, pressure, etc.), we propose and evaluate a control strategy in which the inlet coolant flow rate is cascaded with the average coolant temperature and used for controlling the average solid temperature. In addition, we employ a ratio control strategy, where the inlet molar flow rate of oxygen is used as a dependent manipulated variable and changed in a constant ratio with respect to the inlet molar flow rate of hydrogen. Further, we show that PEMFC does not exhibit a sign change in the gain when the manipulated variables chosen are the inlet molar flow rate of hydrogen and coolant flow (instead of current density/voltage as in [14]). We demonstrate the attainment of improved power densities without having to deal with problems of sign change in gain with this choice of manipulated variables for control of the average power density and the average solid temperature.

The remainder of the paper is structured as follows: Section 2 describes the distributed parameter model for the PEMFC, followed by transient response analysis of the PEMFC for various manipulated variables of interest. Section 3 presents the validation of the PEMFC models against the available literature. Section 4 describes the input–output model for selected manipulated variables and shows that the PEMFC does not exhibit a sign change in gain; also, this section illustrates the design and performance of linear controllers relying on the transfer function models. Finally, we offer conclusions and our plans for future work in Section 5.

2. Mathematical model of the PEMFC

The operating principle of the PEMFC involves the transport of reactants through the electrodes to the reactive sites on the catalyst, where the reaction takes place. The model used in this article is an along-the-channel model developed by Yi and Nguyen [19] and extended by Golbert and Lewin [14]. To avoid dehydration at the anode, the anode stream is saturated with water vapor. The proposed model accounts for (i) the reactions taking place at the anode and cathode, (ii) heat transfer taking place between the solid and the two gas channels, and (iii) heat transfer between the solid and the coolant. The dynamics of the system are captured through the energy balance equation. The electrochemical reactions are known to be faster than the temperature dynamics; hence all other equations except the energy balance are assumed to be at quasi-steady state for a given solid temperature profile.

The consumption equations for the fuel and oxidant are

$$\frac{\mathrm{d}M_{\mathrm{H}_2}(x)}{\mathrm{d}x} = -\frac{h}{2F}I(x) \tag{1}$$

$$\frac{\mathrm{d}M_{\mathrm{O}_2}(x)}{\mathrm{d}x} = -\frac{h}{4F}I(x) \tag{2}$$

Evaporation and condensation influence the balance for liquid water, which is given by

$$\frac{\mathrm{d}M^{\mathrm{l}}_{\mathrm{w},k}(x)}{\mathrm{d}x} = \frac{k_{\mathrm{c}}hd}{RT_k(x)}\left\{\frac{M^{\mathrm{v}}_{\mathrm{w},k}(x)}{\sum_i^{N_k} M_{i,k}}P_k - P^{\mathrm{sat}}_{\mathrm{w}}(T_k)\right\}, \quad k = \mathrm{a}, \mathrm{c} \tag{3}$$

The water vapor flow rates in the channels are affected by various phenomena taking place in the PEMFC, such as (a) water vapor being dragged through the membrane by migrating protons, (b) water being generated due to reaction at the cathode, (c) water vapor diffusing through the membrane, and (d) liquid water condensing and evaporating depending upon the difference in partial pressure and saturation pressure. Based on all these phenomena, the water vapor balance at the anode is given by

$$\frac{dM^{v}_{w,a}(x)}{dx} = -\frac{dM^{l}_{w,a}(x)}{dx} - \frac{h\alpha(x)}{F} I(x) \tag{4}$$

where the first term on the right hand side indicates the rate of evaporation/condensation of the liquid water and the second term is the net amount of water transported across the membrane. The water vapor balance at the cathode is given by

$$\frac{dM^{v}_{w,c}(x)}{dx} = -\frac{dM^{l}_{w,c}(x)}{dx} + \frac{h}{2F} I(x) + \frac{h\alpha(x)}{F} I(x) \tag{5}$$

where the second term on the right hand side indicates the amount of water vapor generated by the reaction at the cathode. The change in temperature of anode gas, cathode gas and coolant are given by

$$\frac{dT_k(x)}{dx} = \frac{U_g A_g \{T_s(x) - T_k(x)\}}{\sum_i C_{p,i} M_i(x)}, \quad k = a, c \tag{6}$$

$$\frac{dT_{cool}(x)}{dx} = \frac{U_w A_{cool} \{T_s(x) - T_{cool}(x)\}}{C_{p,w} M_{cool}} \tag{7}$$

Quantities such as the ratio of water molecules per proton, membrane conductivity and the enthalpy of water evaporation, and their temperature dependency, are specified using empirical equations taken from the work of Golbert and Lewin [14]. These relations are reproduced below.

The ratio of water molecules per proton, α, is given by

$$\alpha = n_d - \frac{F}{I(x)} D^* \frac{dc_w}{dy} - c_w \frac{k_p}{\mu} \frac{F}{I(x)} \frac{dp_w}{dy} \tag{8}$$

The conductivity of the membrane, σ_m, is given as

$$\sigma_m = \left(0.00514 \frac{W_{m,dry}}{\rho_{dry}} c_{w,a} - 0.00326\right) \exp\left(\frac{1}{303} - \frac{1}{T_s}\right) \tag{9}$$

$$D^* = n_d D_0 \exp\left(2416 \left(\frac{1}{303} - \frac{1}{T_s}\right)\right) \tag{10}$$

The enthalpy of water evaporation, $\Delta H_{vap}(T_s)$, is given as

$$\Delta H_{vap}(T_s) = 45,070 - 41.94 T_s + 3.44 \times 10^{-3} T_s^2 + 2.548 \times 10^{-6} T_s^3 - 8.98 \times 10^{-10} T_s^4 \tag{11}$$

The solid temperature of the PEMFC is affected by various mechanisms such as (a) heat transfer by conduction, (b) heat transfer to the fuel and oxidant flows and coolant channels, (c) heat generation by the reactions and (d) heat of evaporation/condensation. The energy balance is given by

$$\rho_s C_{p,s} \frac{\partial T_s}{\partial t} = k_s \frac{\partial^2 T_s}{\partial x^2} + \frac{U_g A_g}{f}(T_a + T_c - 2T_s) + \frac{U_w A_{cool}}{f}(T_{cool} - T_s) - \frac{e}{f}\left(\frac{\Delta H}{2F} + V_{cell}\right) I(x) + \frac{1}{f}\Delta H_{vap}(T_s)\left(\frac{dM^{l}_{w,a}(x)}{dx} + \frac{dM^{l}_{w,c}(x)}{dx}\right) \tag{12}$$

with boundary conditions

$$k_s \frac{\partial T_s}{\partial x}|_{x=0} = U_c(T_s - T_{inf})$$
$$k_s \frac{\partial T_s}{\partial x}|_{x=L} = -U_c(T_s - T_{inf}) \tag{13}$$

The cell voltage is given by

$$V_{cell} = V_{oc} - \eta(x) - \frac{I(x) t_m}{\sigma_m(x)} \tag{14}$$

where the first term on the right side is the open circuit potential, the second term is the activation overpotential and the third term represents ionic resistance.

The Nernst equation is used for calculating the open circuit potential as follows:

$$V_{oc} = V^0_{oc} + \frac{RT_s}{nF} \ln\left(\frac{P_{H_2} P^{0.5}_{O_2}}{P_{H_2O}}\right) \tag{15}$$

However, in the PEMFC, the overpotential mainly occurs at the cathode, so we have

$$I(x) = i_o P_{O_2} \exp\left(\frac{-\alpha F n \eta(x)}{RT_s}\right) \tag{16}$$

and the overpotential is

$$\eta(x) = \frac{RT_s}{F} \ln\left(\frac{I(x)}{i_o P_{O_2}(x)}\right) \tag{17}$$

The voltage obtained from the PEMFC is thus given by

$$V_{cell} = V^0_{oc} + \frac{RT_s}{nF} \ln\left(\frac{P_{H_2} P^{0.5}_{O_2}}{P_{H_2O}}\right) - \frac{RT_s}{F} \ln\left(\frac{I(x)}{i_o P_{O_2}(x)}\right) - \frac{I(x) t_m}{\sigma_m(x)} \tag{18}$$

2.1. Solution procedure

The data for the base case considered in this paper is given in Table 1. The modeling equations are solved along the channel. Eq. (18) is solved for current density after setting the cell voltage. After obtaining the current density, the quasi-steady state equations (Eqs. (1)–(7)) are integrated along the channel (in the positive x-direction) by using a differential equation solver. Here, it is important to note that Eq. (3) is used only when liquid water is present at the cathode or anode and/or the partial pressure is greater than the saturation pressure of water vapor.

Table 1
Data for the base case

Input variable	Value
M_{H_2} (mol s^{-1})	1.14×10^{-5}
M_{O_2} (mol s^{-1})	5.7×10^{-6}
$M^{v}_{w,a}$ (mol s^{-1})	9.8555×10^{-6}
$M^{v}_{w,c}$ (mol s^{-1})	8.855×10^{-6}
$M^{l}_{w,a}$ (mol s^{-1})	0
$M^{l}_{w,c}$ (mol s^{-1})	0
T_a (K)	353
T_c (K)	353
T_{cool} (K)	340
T_{inf} (K)	343
P_a (atm)	1
P_c (atm)	1

This type of situation has been handled in MATLAB using the EVENT function. In the present work, the PEMFC is operated on pure hydrogen and pure oxygen at the anode and cathode, respectively.

The energy balance equation, which captures the dynamics of the system, is discretized using the Crank–Nicholson method as given in Golbert and Lewin [14]. The set of algebraic equations obtained by discretizing the energy balance equation along the channel are solved to obtain the solid temperature profile for the next time instant.

2.2. Empirical identification of PEMFC dynamics

In this section, we present methods that were used to identify reduced order models that were subsequently used in control structure analysis and also for controller design. From a control viewpoint, the PEMFC is considered as a MIMO system, where the average power density and average solid temperature are the two outputs to be controlled. The inlet molar flow rates of oxygen and hydrogen, inlet temperatures of anode and cathode gas, and the inlet coolant flow rate are considered as possible manipulated variables.

To obtain a reduced order representation of the dynamics of the system, we perform step changes on all the above-mentioned manipulated variables as follows.

2.2.1. Response to a step change in the molar flow rate of hydrogen

Fig. 1 shows the dynamic response of the average power density and average solid temperature to step changes in the inlet molar flow rate of hydrogen. The hydrogen stream is saturated with water vapor at the inlet. When the flow rate of hydrogen is increased, we observe an instant increase and then a relatively slower, small decrease in the average power density. The instant shoot-up is because of an increase in the conductivity of the membrane [20] (caused by the larger amount of water brought in by the hydrogen), which results in a higher current density downstream in the channel. This increased current density results in a higher consumption of oxygen, which decreases its partial pressure and results in an increase in the activation overpotential. Due to this increase in the activation overpotential, the current density decreases, resulting in a slight decrease in the power density. Also, due to an increase in the rate of reaction, the average solid temperature increases.

2.2.2. Response to a step change in the molar flow rate of oxygen

Fig. 2 shows the dynamic response of the average power density and average solid temperature to step changes in the

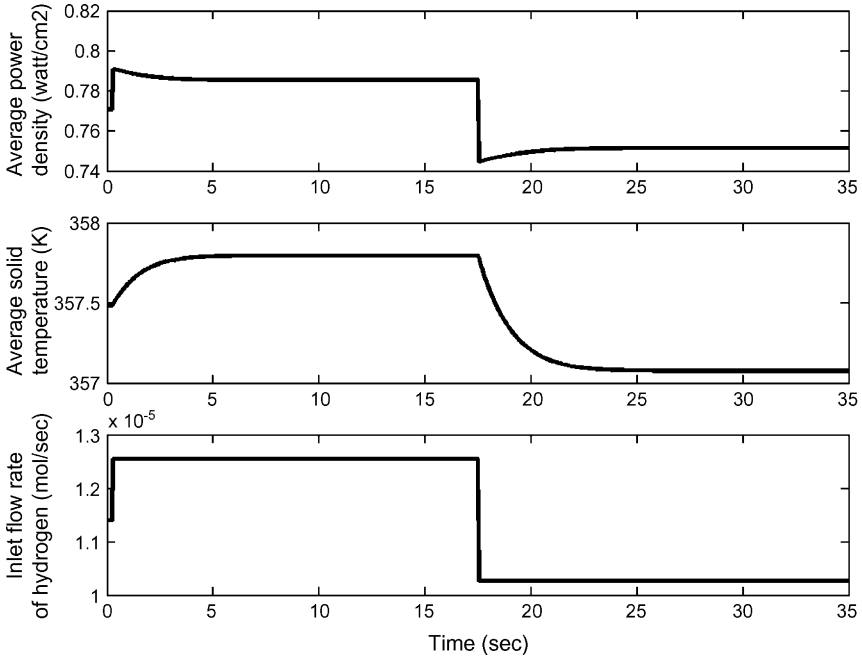

Fig. 1. Step response of the average power density and average solid temperature to changes in the inlet molar flow rate of hydrogen.

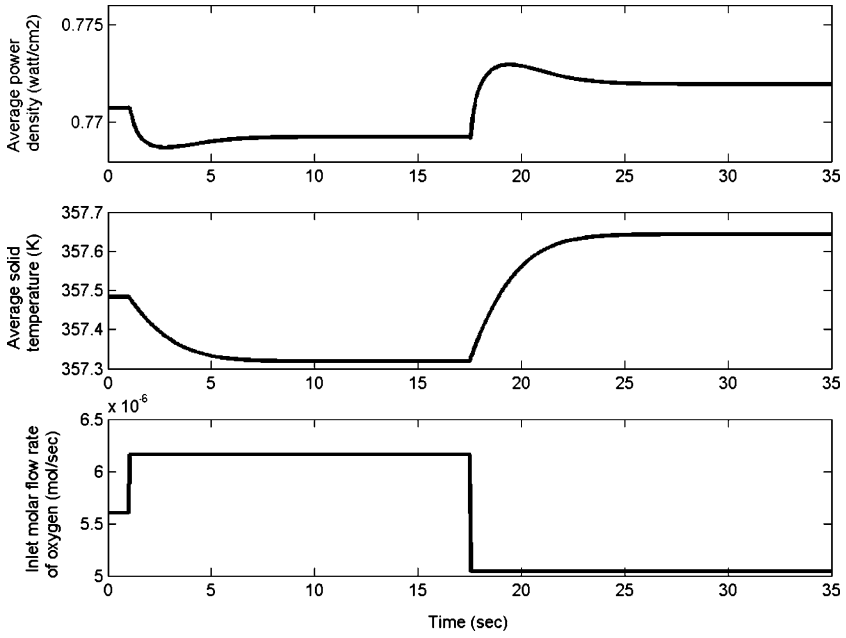

Fig. 2. Step response of the average power density and average solid temperature to changes in the inlet molar flow rate of oxygen.

inlet molar flow rate of oxygen. Due to an increase in the molar flow rate of oxygen, the partial pressure of water vapor at the cathode decreases, which results in a decrease in the rate of water condensation, and hence a small amount of heat is released. Due to this, the average solid temperature decreases and the overall effect is to decrease the average power density. When the step change is given, we observe a small inverse response immediately after, which can be explained in terms of lead–lag behavior. The lead behavior is due to a decrease in the activation overpotential, and the lag-like behavior is due to a decrease in the solid temperature.

2.2.3. Response to a step change in the inlet anode gas temperature

Fig. 3 shows the dynamic response of the average power density and the average solid temperature to step changes in the inlet anode gas temperature. The initial increase in power density results from an increase in the current density along the channel. The current density increases because the ionic resistance decreases due to an increase in the membrane conductivity. The membrane conductivity increases because an increase in partial pressure of water vapor takes place, as the gas at the anode is saturated. But due to an increase in the solid temperature,

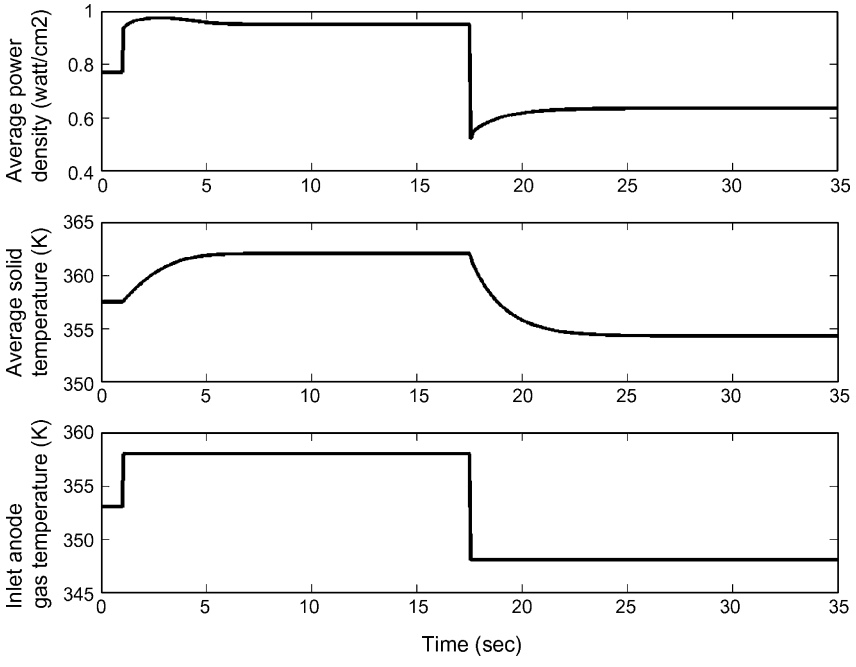

Fig. 3. Step response of the average power density and average solid temperature to changes in the inlet anode gas temperature.

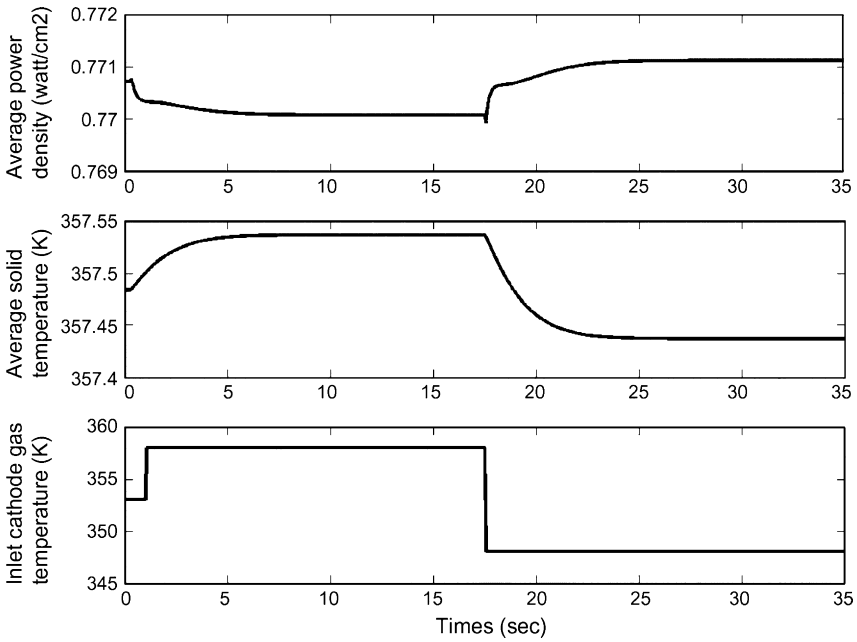

Fig. 4. Step response of the average power density and average solid temperature to changes in the inlet cathode gas temperature.

there is a decrease in the membrane conductivity. Though these two conflicting phenomena take place simultaneously, there is a net increase in the membrane conductivity, which results in an increase in the current density. The high current density along the channels results in an increase in the average solid temperature.

2.2.4. *Response to a step change in the inlet cathode temperature*

Fig. 4 shows the dynamic response of the average power density and average solid temperature to step changes in the inlet cathode gas temperature. Due to an increase in the cathode gas temperature, the saturation pressure at the cathode increases and the driving force for the condensation decreases; this results in an increase in the partial pressure of water vapor and a decrease in the partial pressure of oxygen. Due to this effect, the concentration term in Eq. (18) and the activation overpotential become dominant, and hence the power density decreases. The small inverse response in the average power density can again be explained in a manner similar to that for the step change in the oxygen flow rate. Also, as the inlet gas temperature increases, more heat enters into the system, which results in an increase in the solid temperature.

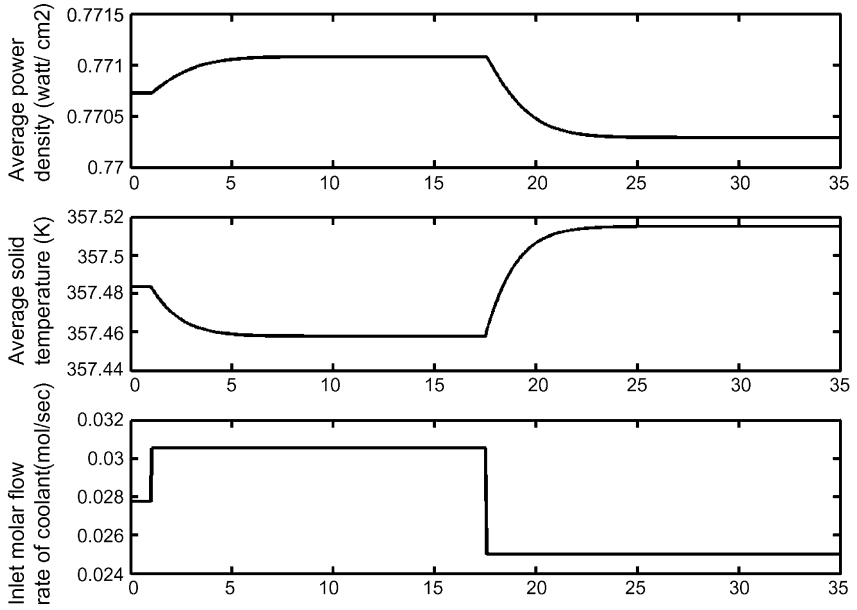

Fig. 5. Step response of the average power density and average solid temperature to changes in the inlet molar flow rate of coolant.

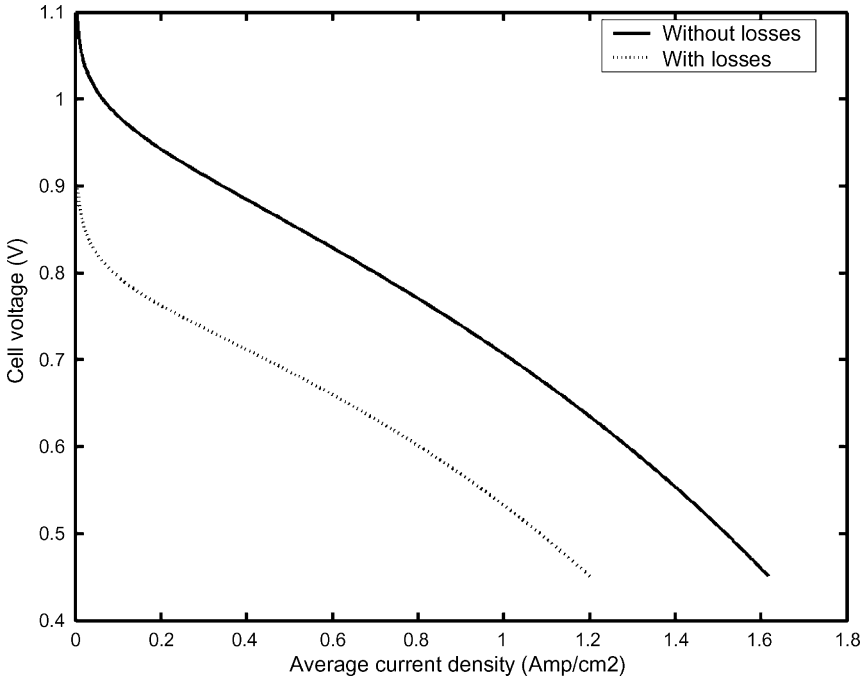

Fig. 6. Comparison of polarization curves with and without losses due to effects such as catalyst corrosion and electrical shorting.

2.2.5. Response to a step change in the molar flow rate of coolant

Fig. 5 shows the dynamic response of the average power density and average solid temperature to step changes in the inlet molar flow rate of coolant. The figure shows a decrease in the average solid temperature when the coolant flow is increased, which can be explained in terms of increased heat transfer to the coolant. Due to the decrease in the average solid temperature, the conductivity of the membrane increases and the ionic resistance decreases. Due to this decrease in the ionic resistance, the current density increases, and this results in an increase in the average power density.

3. Model validation

The distributed parameter model of the PEMFC is validated by plotting the polarization curve of the PEMFC. This polarization curve shows good qualitative agreement with polarization curves provided in the literature (Ceraolo et al. [1], and references with in). In our model, we have neglected phenomena such

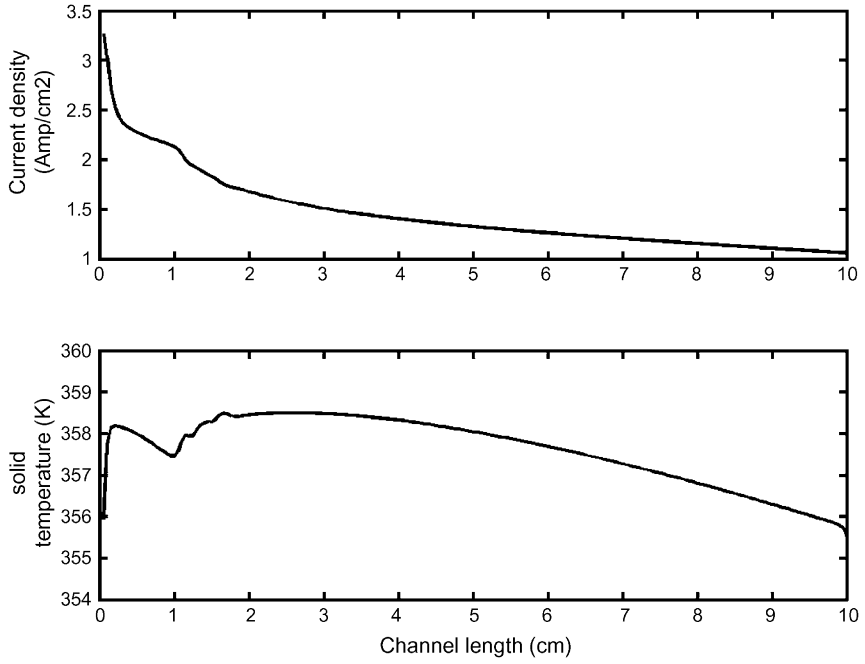

Fig. 7. Prediction of steady-state current density and solid temperature along the channel (good qualitative agreement with Yi and Nguyen [19]).

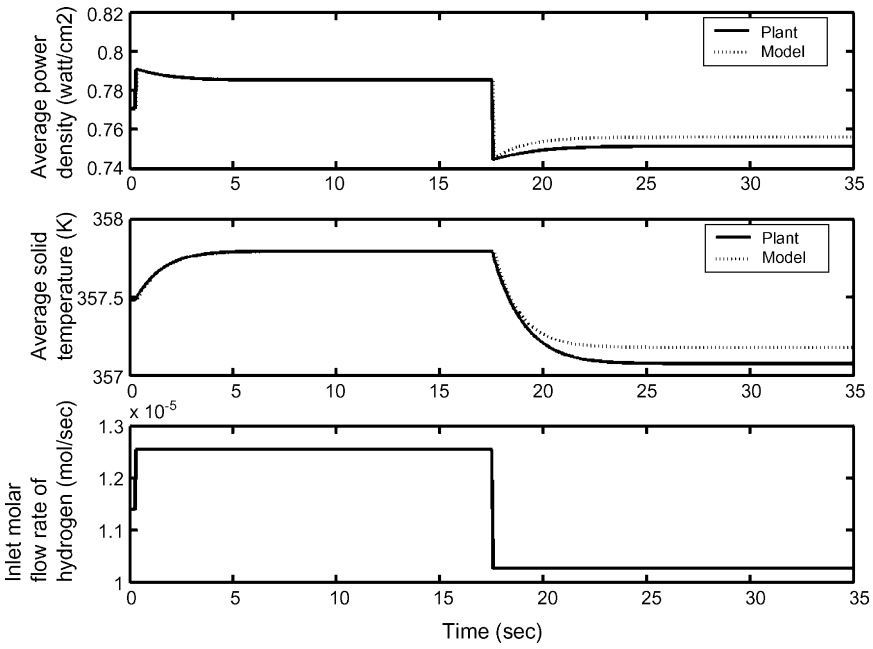

Fig. 8. Empirical model validation of response to step in the inlet molar flow rate of hydrogen.

as inter-diffusion of reactant gases through the membrane, catalyst corrosion or electric shorting, which result in losses in the open circuit potential. Considering these losses to be ∼200 mV, we have constructed another polarization curve, and have found the power density to be approximately 20–30% lower. These polarization curves are shown in Fig. 6. In our control simulations, we have neglected the effect of these losses.

3.1. PEMFC model validation

The PEMFC model operating on pure oxygen at the cathode is also qualitatively validated against the available literature, specifically with the work of Yi and Nguyen [19]. We have compared the spatial variation of current density and solid temperature of the PEMFC at steady-state with their results. The graphs are illustrated in Fig. 7, which shows good agreement with the work of Yi and Nguyen [19].

3.2. Empirical model validation

We have generated empirical models for the purpose of controller design. These empirical models were obtained by fitting transfer function models to the step responses for various manipulated variables such as inlet molar flow rate of hydrogen,

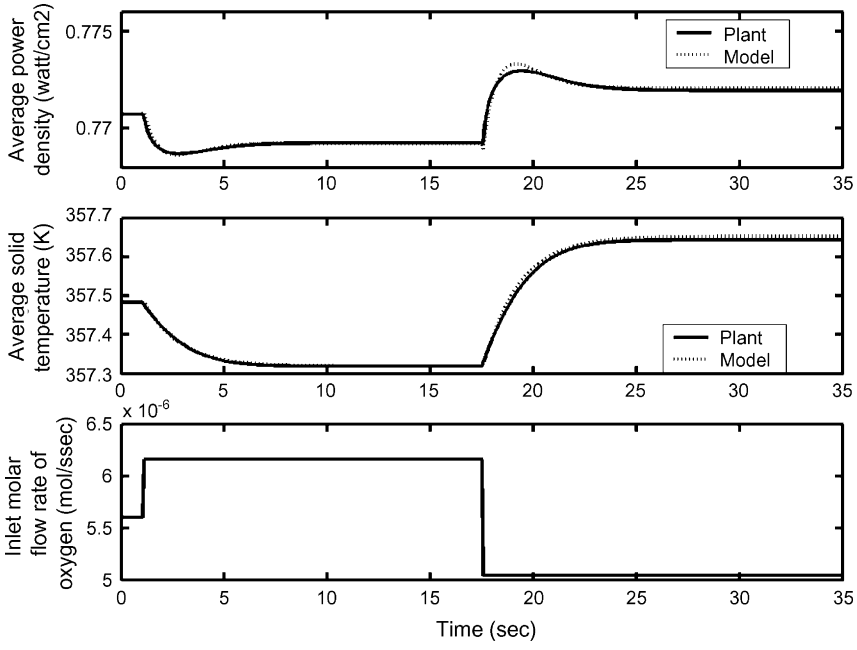

Fig. 9. Empirical model validation of response to step in the inlet molar flow rate of oxygen.

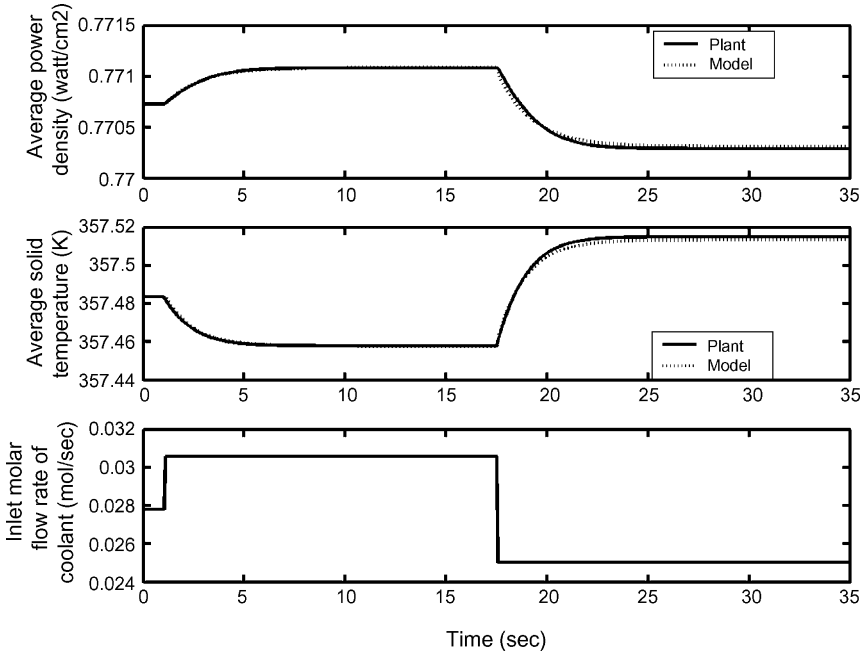

Fig. 10. Empirical model validation of response to step in the inlet molar flow rate of coolant.

oxygen and coolant. The validation of these models against the step responses obtained from the nonlinear distributed PEMFC model is given in Figs. 8–10. The empirical models show good fits with the nonlinear models for positive and negative step changes in the manipulated variables. There is a slight inaccuracy in the model with inlet molar flow rate of hydrogen for negative step changes (due to non-symmetric nonlinearity).

4. Linear control of the PEMFC

The power density is the important output of interest from any type of fuel cell. To obtain maximum power density from a fuel cell, a robust control strategy is needed. The PEMFC offers many challenges for controller design such as sign change in the gain of the plant, severe nonlinearities, and possible starvation of reactants. Golbert and Lewin [14] state that the maximum power density obtained by linear controllers from PEMFC is limited, since linear controllers cannot handle the change in the sign of the gain. However, this problem can be avoided by carrying out proper selection of the manipulated variables, as shown in Section 4.1.

As stated earlier, the PEMFC is considered here to be a MIMO system; the controlled outputs are the average power density and the average solid temperature. To control those outputs, various manipulated variables such as the inlet molar flow rates of oxygen and hydrogen, inlet anode and cathode gas temperatures and inlet coolant flow rate are available. Of these, certain variables such as the inlet coolant temperature make poor choices as manipulated variables because they add the cost of extra hardware and make the system more complex.

To select suitable manipulated variables for controlling average power density and average solid temperature, we have carried out an analysis of the steady-state relative gain array (RGA). The operating conditions for the RGA are the base case conditions presented in Table 1. The procedure for finding the elements of the RGA matrix and prediction of interactive effects are given in Appendix A. Pairs of possible manipulated variables were chosen, and step changes in the manipulated variables were implemented as described in the earlier section, and empirical dynamic models were identified. These empirical dynamics models were validated for step changes in both directions as shown in Section 3.2, and are shown in Table 2. A representa-

Table 2
Empirical dynamic models

Empirical dynamic model	Parameters
$\frac{y_1}{m_1} = k_1 - \frac{k_2(1-\eta s)}{\tau s+1}$	$k_1 = 17{,}680$, $k_2 = 4845$, $\eta = 0.01$, $\tau = 1.5$
$\frac{y_1}{m_2} = \frac{k_1(1-\eta s)(\tau s+1)}{\tau_1^2 s^2 + 2\xi\tau_1 s + 1}$	$k_1 = -2.653\text{e}3$, $\eta = 0.01$, $\tau = 2.5$, $\tau_1 = 0.9747$, $\xi = 1.7875$
$\frac{y_1}{m_3} = k_1 + \frac{k_2}{\tau^2 s^2 + 2\xi\tau s + 1}$	$k_1 = 0.006$, $k_2 = 0.03$, $\tau = 1.07$, $\xi = 0.411$
$\frac{y_1}{m_4} = \frac{k_1(1-\eta s)(\tau s+1)}{\tau_1^2 s^2 + 2\xi\tau_1 s + 1}$	$k_1 = -1.28\text{e}{-4}$, $\eta = 0.03$, $\tau = 2.5$, $\tau_1 = 0.9747$, $\xi = 3.7875$
$\frac{y_1}{m_5} = \frac{k_1}{\tau s+1}$	$k_1 = 0.1287$, $\tau = 1.7$
$\frac{y_2}{m_1} = \frac{k_1}{\tau s+1}$	$k_1 = 2.735\text{e}5$, $\tau = 1.2$
$\frac{y_2}{m_2} = \frac{k_1}{\tau s+1}$	$k_1 = -2.9375\text{e}5$, $\tau = 1.7$
$\frac{y_2}{m_3} = \frac{k_1}{\tau s+1}$	$k_1 = 0.9093$, $\tau = 1.4$
$\frac{y_2}{m_4} = \frac{k_1(1-\eta s)}{\tau s+1}$	$k_1 = 0.0107$, $\tau = 1.6$
$\frac{y_2}{m_5} = \frac{k_1}{\tau s+1}$	$k_1 = -9.2806$, $\tau = 1.4$

y_1: average power density; y_2: average solid temperature; m_1: inlet molar flow rate of hydrogen; m_2: inlet molar flow rate of oxygen; m_3: inlet gas temperature at anode; m_4: inlet gas temperature at cathode; m_5: Inlet molar flow rate of coolant.

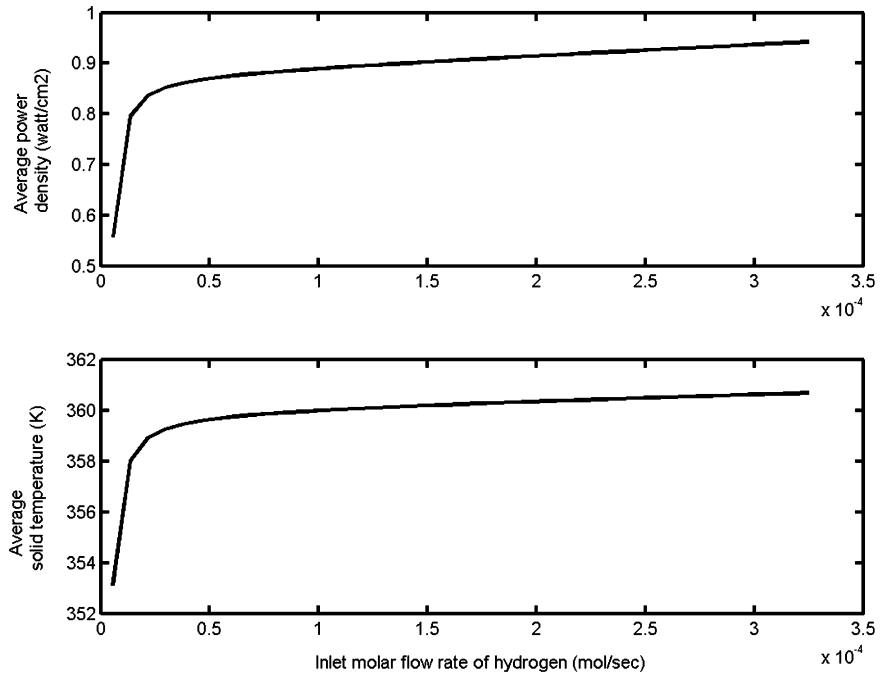

Fig. 11. Steady-state input–output relationship between the average power density/average solid temperature and the inlet molar flow rate of hydrogen.

tive RGA matrix for average power density and average solid temperature as the outputs with inlet molar flow rate of hydrogen and the coolant as inputs is

$$(\mathrm{RGA})_{y_1y_2,m_1m_5} = \begin{bmatrix} 0.7718 & 0.2281 \\ 0.2281 & 0.7718 \end{bmatrix} \tag{19}$$

For the rest of the manipulated variables, the RGA matrices are given in Appendix A. It can be seen that for some of the pairings (notably $y_1, y_2 \rightarrow m_2, m_4$ and $y_1, y_2 \rightarrow m_3, m_5$), the presence of interaction is quite significant. However, the elements of the RGA matrix for the chosen pairing above suggest that there are minimal interactions between these two control loops, and the inlet molar flow rate of hydrogen and inlet molar flow rate of coolant can therefore be selected as manipulated variables for controlling the desired outputs of the PEMFC.

4.1. Input–output model at steady-state

We present results for the change in outputs due to changes in the manipulated variables selected using RGA in this subsection. In these simulations, the PEMFC was initially maintained at the

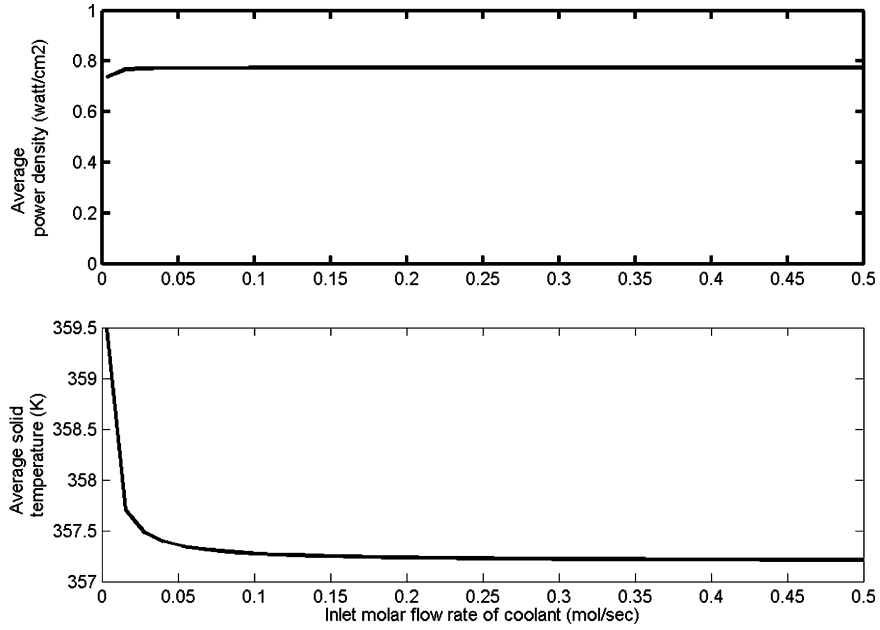

Fig. 12. Steady-state input–output relationship between the average power density/average solid temperature and the inlet molar flow rate of coolant.

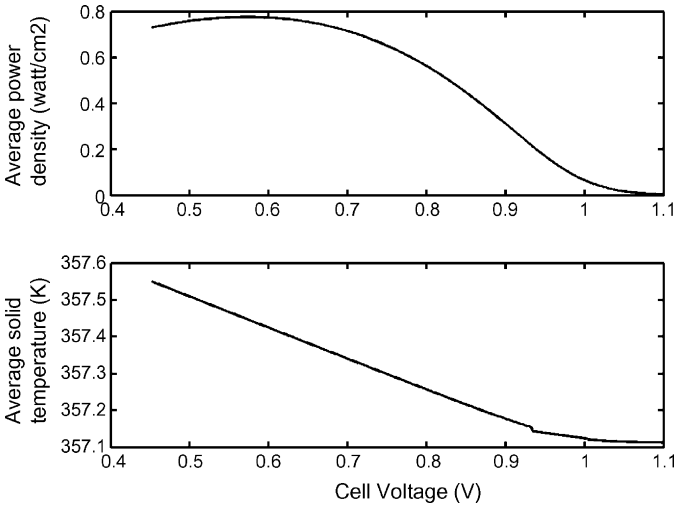

Fig. 13. Steady-state input–output relationship between the average power density/average solid temperature and the cell voltage.

base case steady-state temperature, and the selected manipulated variable was changed keeping all other operating conditions the same as in the base case. Fig. 11 shows that the average power density and average solid temperature exhibit a positive gain with respect to the inlet molar flow rate of hydrogen, over a wide range of average power densities. Fig. 12 illustrates that the inlet molar flow rate of coolant has negligible effect on the average power density, but the average solid temperature exhibits a negative gain with respect to the coolant flow. Fig. 13 depicts the sign change in gain of average power density with cell voltage. Fig. 13 also helps in qualitatively validating our PEMFC model with the existing literature, especially the work of Golbert and Lewin [14].

To select a particular set point for current density and associated power density, a pure resistive load is connected across the fuel cell. The pure resistive load loop is assumed to be ideal, so that it does not involve any kind of dynamics but only the calculation of the desired current density and associated power density.

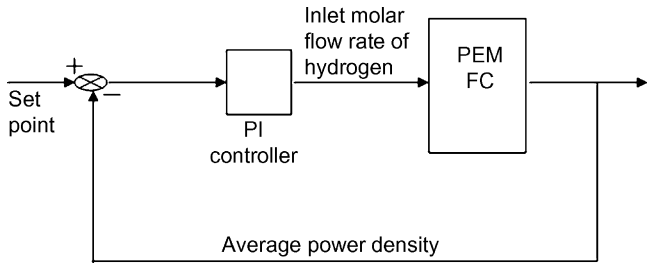

Fig. 14. Schematic of power control loop using inlet molar flow rate of hydrogen as the manipulated variable.

4.2. Power control loop

For the power control loop, the average power density in the PEMFC was controlled by manipulating the inlet molar flow rate of hydrogen, as in [16]. Here, we additionally evaluate and compare the use of the oxygen molar flow rate as a manipulated variable. The following subsections describe the performance of the individual control loops.

4.2.1. Using inlet molar flow rate of hydrogen

The controller for the hydrogen flow → power density loop is designed by using the internal model control (IMC) based PID method. The empirical transfer function models developed earlier and presented in Table 2 are used for the design. The block diagram of the control system is shown in Fig. 14. The resulting controller is of PI form and its parameters are shown in Table 3. The performance of the PI controller along with the manipulated variable actions is shown in Fig. 15. The set-

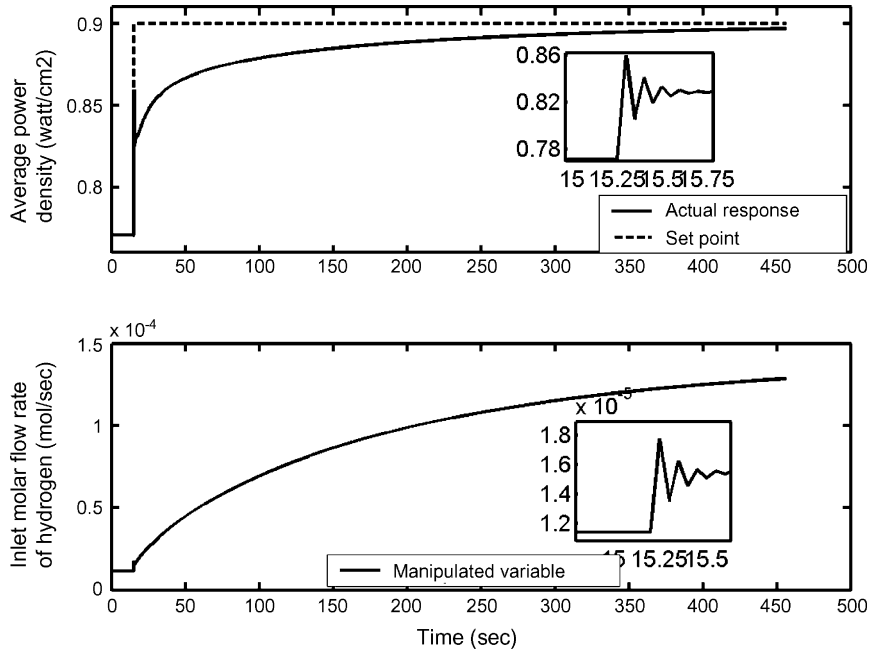

Fig. 15. Performance of the power control loop using the inlet molar flow rate of hydrogen as the manipulated variable.

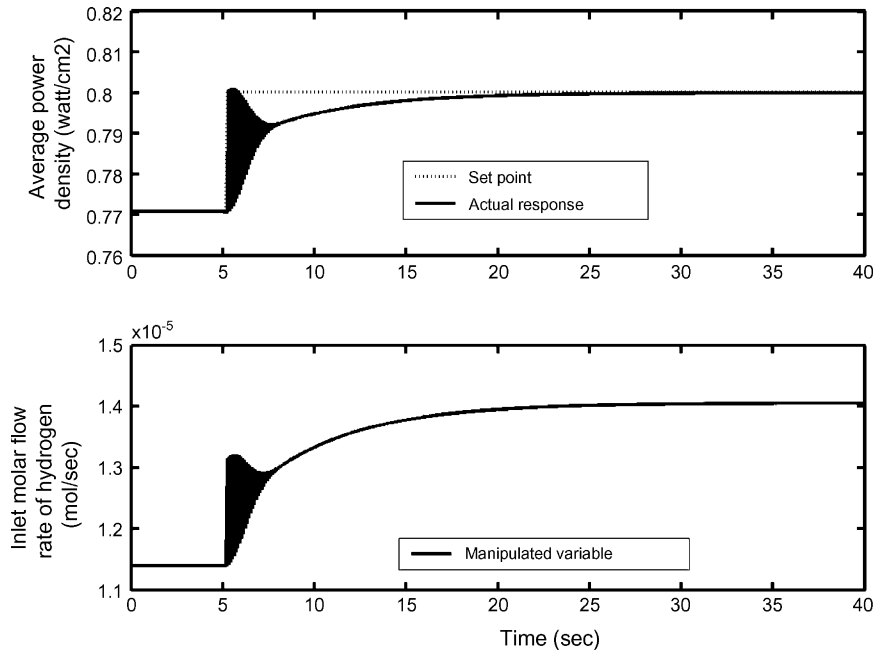

Fig. 16. Performance of power control loop for small deviation in set point from steady-state set point using the inlet molar flow rate of hydrogen as the manipulated variable. The quicker response time illustrates nonlinearities in the power control loop.

tling time for this control strategy is approximately 275 s. This large settling time could be attributed to severe nonlinearities present in the PEMFC. To verify that the linear controller performance was indeed poor due to the presence of nonlinearities, we further performed two simulations as follows: (1) A relatively smaller deviation in the set point (set point changed to 0.8 W cm^{-2}) was specified and the performance of the controller was compared (Fig. 16). It can be seen from Fig. 16 that the settling time of this controller was approximately 11.5 s, which is significantly smaller than the settling time with a specified set point of 0.9 W cm^{-2}; this behavior clearly indicated the existence of an input dependent nonlinearity. (2) In the second simulation, the nonlinear PEMFC plant was replaced with the linear empirically identified model (transfer function model) as shown in Table 2, and the performance of this linear controller with this linear plant was again compared. As shown in Fig. 17, the settling time for this linear control is approximately 10 s. Also, there were no oscillations in the initial response. From these two simulations, it can be concluded that the large settling time for the power control loop is due to the presence of

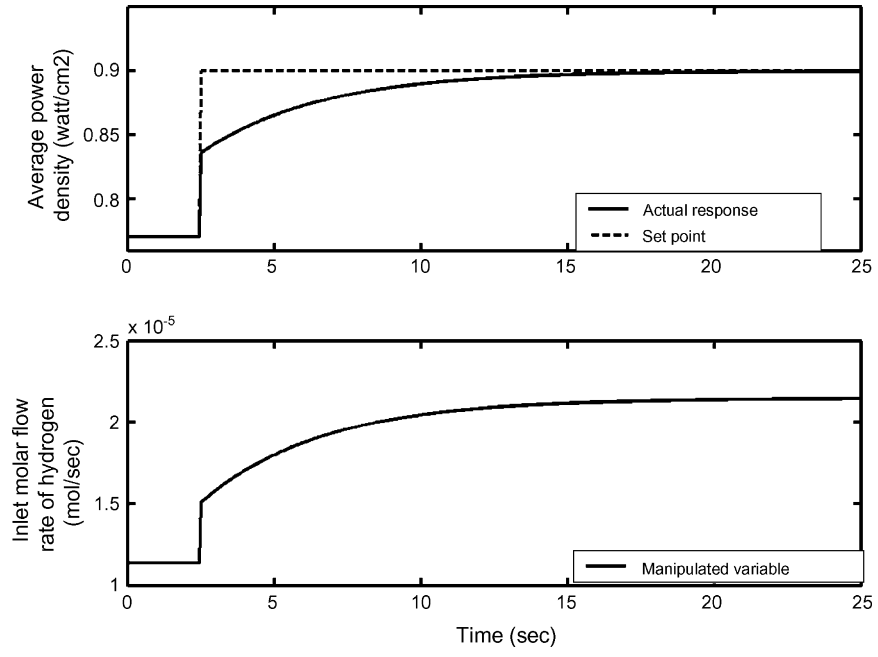

Fig. 17. Performance of linear empirical identified model (transfer function) in power control loop using inlet molar flow rate of hydrogen as the manipulated variable.

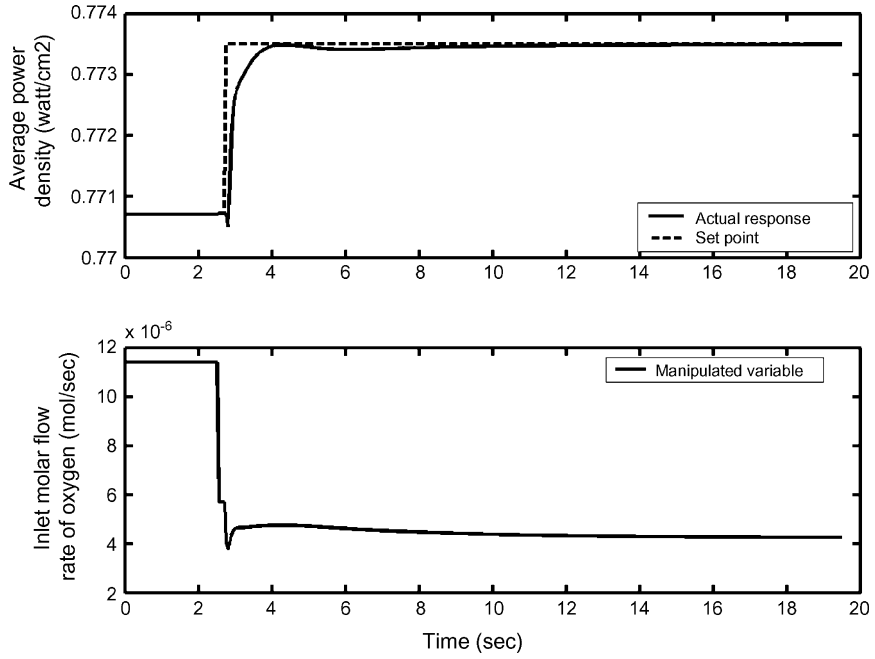

Fig. 18. Performance of the power control loop using the inlet molar flow rate of oxygen as the manipulated variable.

nonlinear dynamics in the PEMFC, and therefore a linear controller would be expected to have limitations on closed loop performance.

4.2.2. Using the inlet molar flow rate of oxygen

This IMC-PID controller is designed using the same method as for the hydrogen flow rate based controller, and the details are shown in Table 3. The performance of this control loop is shown in Fig. 18. The dynamic closed loop response is faster than in the case when the hydrogen flow rate is used as the manipulated variable. However, as shown in Section 2, the power density has a negative gain with respect to the oxygen flow rate. This means that to obtain higher power density, low oxygen flow rates are required, which brings in the possibility of oxygen starvation. Thus, the inlet molar flow rate of oxygen is not a feasible manipulated variable for controlling the power density. For the base

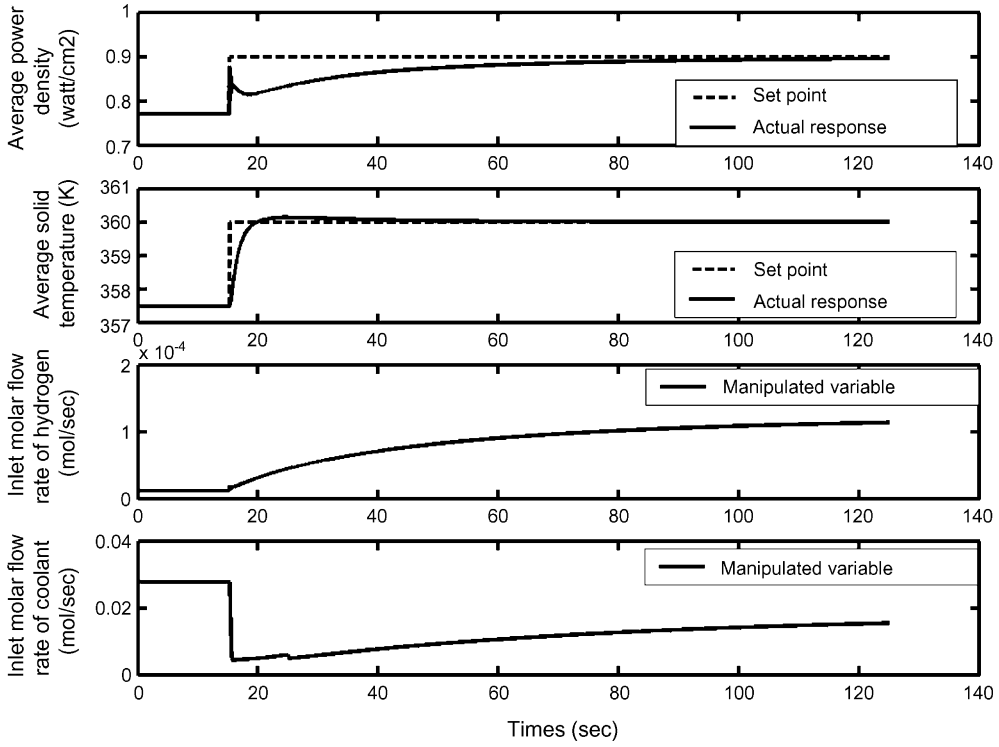

Fig. 19. Performance of the cascade controller in rejecting the disturbance introduced in the inlet coolant temperature.

Table 3
Design parameters for various control strategies studied

Controller	Manipulated variable	K_{cc}	τ_I	τ_D
Power control loop	Inlet molar flow rate of hydrogen	5.743e−5	1.5	
	Inlet molar flow rate of oxygen	−6.5746e−4	3.1	0
Cascade control loop				
Outer loop	Inlet molar flow rate of coolant	0.75	1.5	
Inner loop	Inlet coolant temperature	−0.0333	0.75	
Ratio control loop	Inlet molar flow rate of hydrogen	5.743e−5	1.5	

The general form of PID controller is given as: $G_c(s) = K_{cc}(1 + (1/\tau_I s) + (\tau_D s))$.

case shown in Table 1, the maximum achievable power density using the inlet molar flow rate of oxygen is 0.7736 W cm^{-2}.

4.3. Power and solid temperature control loop

4.3.1. Cascade control for solid temperature

To achieve maximum power density, the rate of reaction needs to be maintained at a high value. Due to the increased rate of reaction, the heat produced from the reaction is large, which increases the solid temperature of the PEMFC. Increasing the solid temperature beyond the specific value will adversely affect the conductivity of the membrane and also the catalyst activity, which in turns affects the rate of reaction. Hence, it is necessary to control the average solid temperature within specified limits. To control the average solid temperature, the RGA analysis shown in Appendix A recommends the inlet coolant flow rate to be the manipulated variable. The average solid temperature can be controlled by using a feedback control loop with the inlet molar flow rate of coolant as the manipulated variable, but we use a cascade control loop in this study.

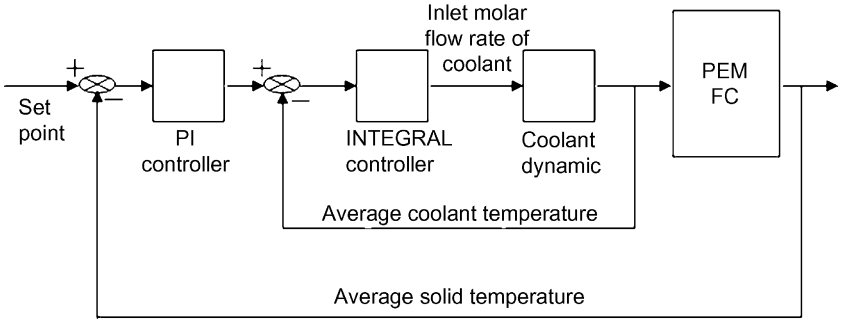

Fig. 20. Schematic of the cascade control loop using inlet molar flow rate of coolant as the manipulated variable.

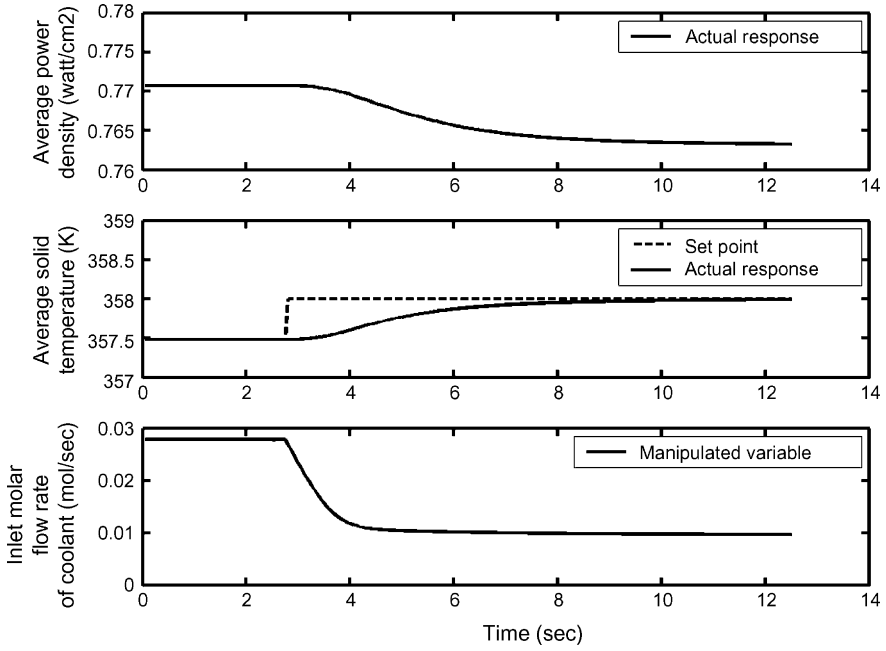

Fig. 21. Performance of cascade control using the inlet molar flow rate of coolant as the manipulated variable.

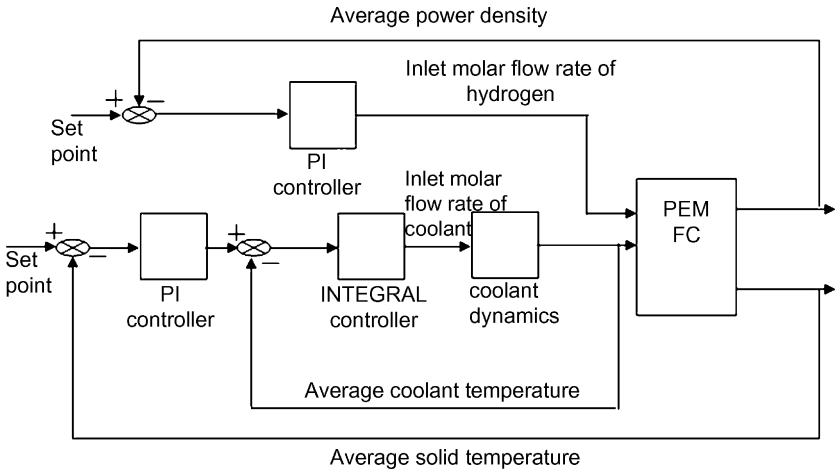

Fig. 22. MIMO control schematic.

As compared to the simple feedback control loop, this strategy provides the additional advantage of disturbance rejection. Fig. 19 shows the performance of the cascade control loop while rejecting a disturbance in the inlet coolant temperature. The cascade control schematic is shown in Fig. 20. The servo (set point tracking) performance of this control strategy is shown in Fig. 21.

As explained in Section 4.2.2, the power control loop that manipulates the oxygen flow fails to satisfy large power density demand; also, with hydrogen flow as the manipulated variable, the solid temperature rise is high in the PEMFC. Therefore, to obtain higher power densities with hydrogen, the solid temperature should be controlled along with the average power density. Controlling the solid temperature at a lower value will also avoid unwanted problems such as decrease in conductivity and deactivation of catalyst [20]. This resulting multivariable controller strategy is discussed in the next subsection.

4.3.2. MIMO control strategy

The MIMO control strategy is shown in Fig. 22 and its performance in Fig. 23. Fig. 23 shows that the response of the MIMO controller is faster than that of the SISO controller. The settling time for the MIMO controller is approximately 90 s and that for the SISO controller is 275 s. It can be seen that by controlling the average solid temperature along with the average power density, faster responses can be obtained when compared to the SISO controller case; the unwanted effect of rise in temperature is also avoided. We have also carried out a simulation using air instead of oxygen at the cathode, and its performance shown in Fig. 24. The results demonstrate that the MIMO control strategy

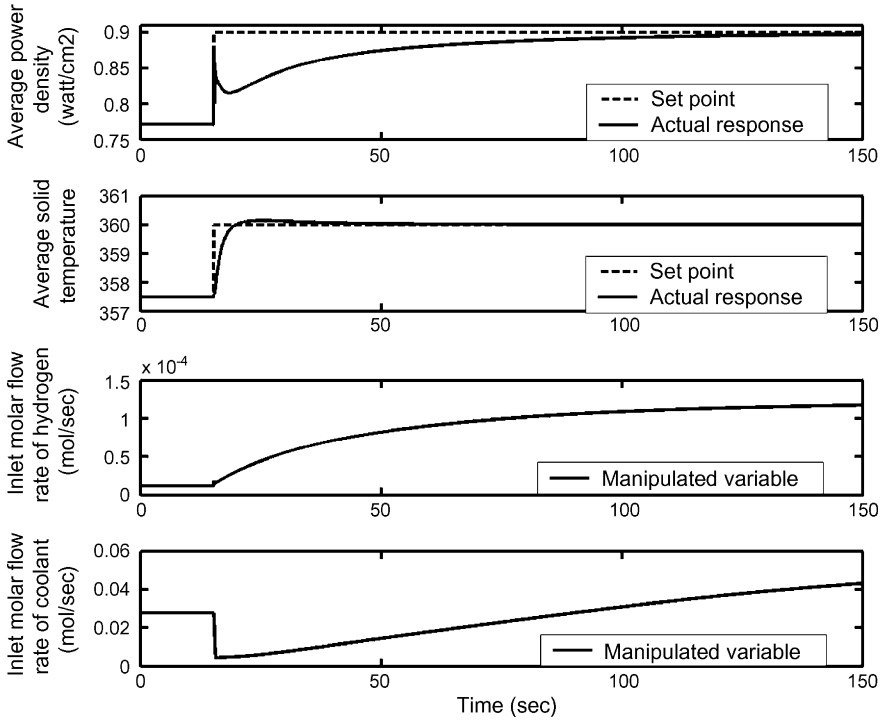

Fig. 23. Performance of the proposed MIMO control strategy in response to changes in the set points for the average power density and the average solid temperature.

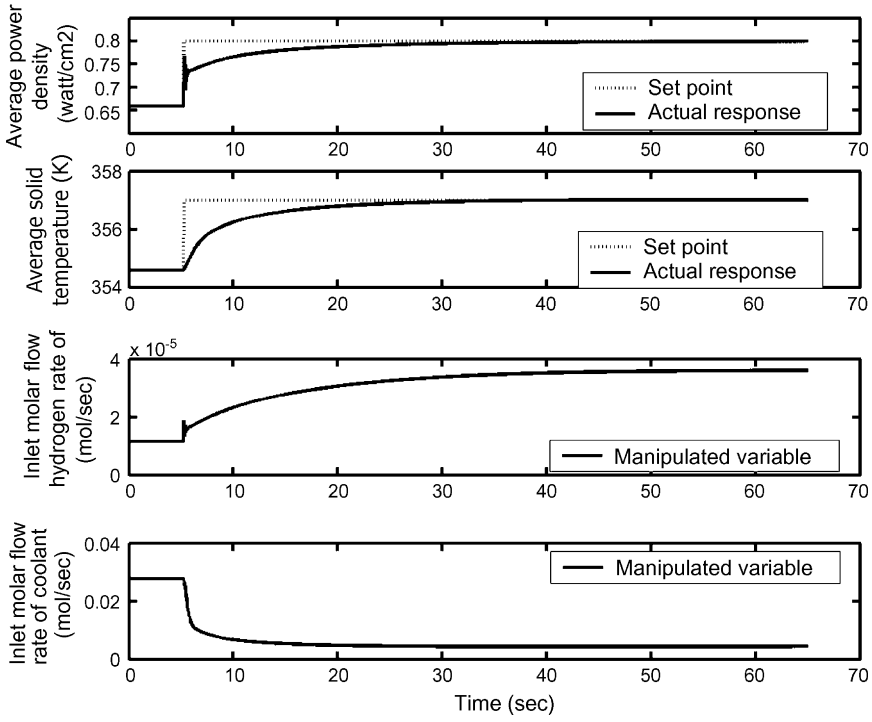

Fig. 24. Performance of the proposed MIMO control strategy in response to changes in the set points for the average power density and the average solid temperature using air at the cathode.

can provide satisfactory control performance for hydrogen–air fuel cells.

When a higher power density is required from the PEMFC, it is expected that the consumption of reactant would increase. In the MIMO control strategy, the input molar flow rate of hydrogen is used as the manipulated variable. However, there is no control on the input molar flow rate of oxygen and hence this control strategy is vulnerable to the problem of oxygen starvation at high power densities. Fig. 25 shows the output flow rate of oxygen from the PEMFC for the MIMO control strategy. The output flow rate decreases with time, which indicates that for higher power density demand, the PEMFC will face the problem of oxygen starvation. In this paper, we also recommend the use of a ratio strategy to avoid this oxygen starvation. We discuss these results in next subsection.

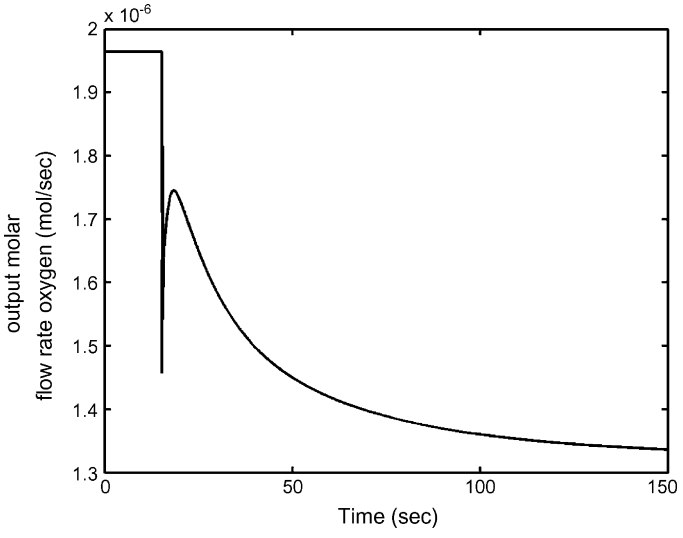

Fig. 25. Output flow rate of oxygen from the PEMFC with MIMO control, corresponding to the results shown in Fig. 23.

4.4. Ratio control

We have implemented a ratio control strategy to avoid the problem of oxygen starvation and satisfy maximum power density demand. A schematic for this strategy is shown in Fig. 26. In this strategy, the measured manipulated variable is the inlet molar flow rate of hydrogen, because the average power density has a positive gain with respect to it. The inlet flow rate of oxygen is changed in proportion with the inlet flow rate of hydrogen. The stoichiometric requirement of ratio of inlet molar flow rate of hydrogen to oxygen is 2; however, keeping in view the parasitic requirements of the power necessary for pumping oxygen, we have used a value of 8 for this ratio. This higher ratio could cause starvation immediately after the positive set point change for average power density has been made. To avoid this, the inlet molar flow rate of oxygen is initially kept constant at a minimum value. Once the hydrogen flow rate increases in response to the step change, the oxygen flow rate recommended by the ratio controller will rise above this minimum value. From this point on, the oxygen flow rate specified by the controller will be the value calculated using the ratio of 8. For higher power density demand, a higher flow rate of hydrogen is required which will ultimately increase the molar flow rate of oxygen and overcome the problem of oxygen starvation. The performance of the ratio control strategy is shown in Fig. 27. To improve the performance of ratio control, the average solid temperature is also controlled using

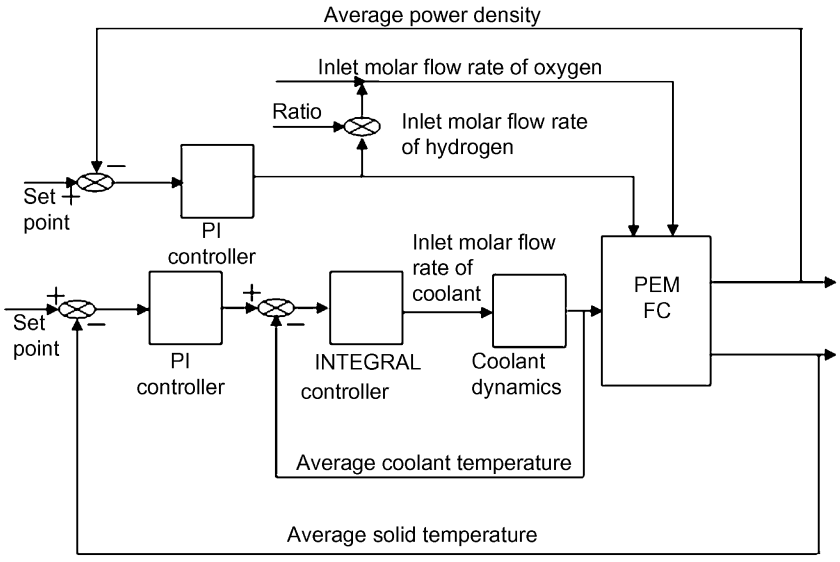

Fig. 26. Schematic for ratio control along with cascade control for temperature.

the previously described cascade control strategy. The response of this ratio controller is faster than the MIMO strategy using only hydrogen as the manipulated variable. The ratio controller is faster because on loop closure, the initial input molar flow rate of oxygen is lower than that of the base case flow rate. As explained above, the input molar flow rate of oxygen shows negative gain with average power density and hence this lower molar flow rate of oxygen helps in achieving maximum average

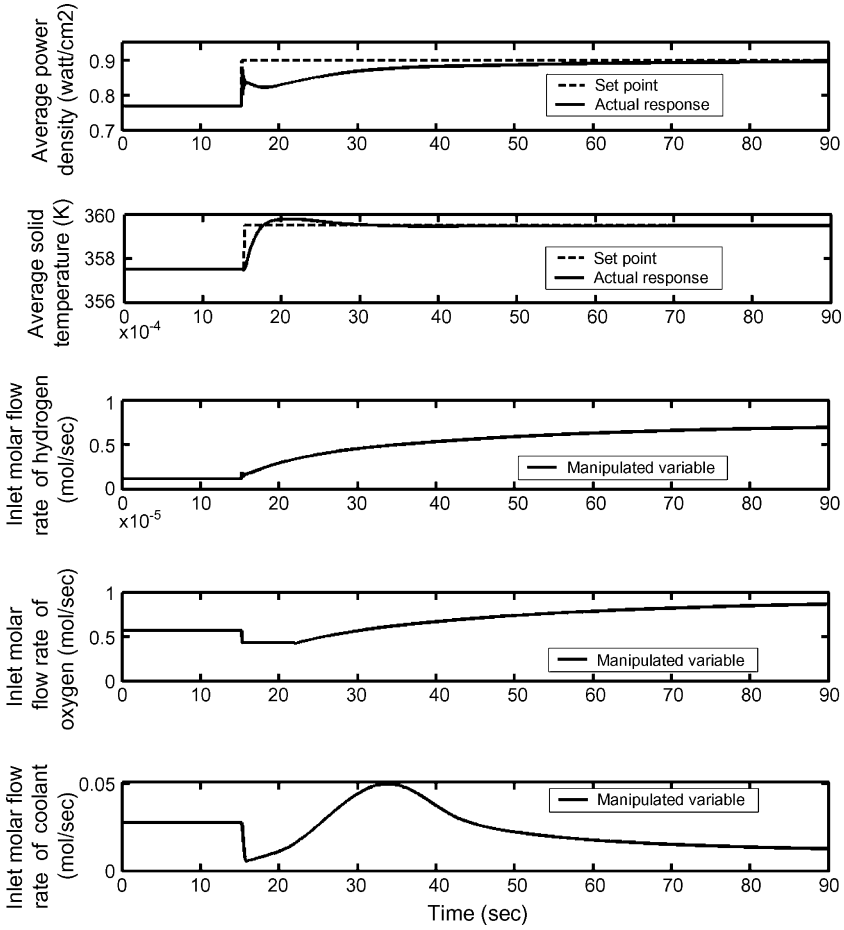

Fig. 27. Performance of the multivariable controller with ratio control for oxygen in response to changes in the set points of the average power density and the average solid temperature.

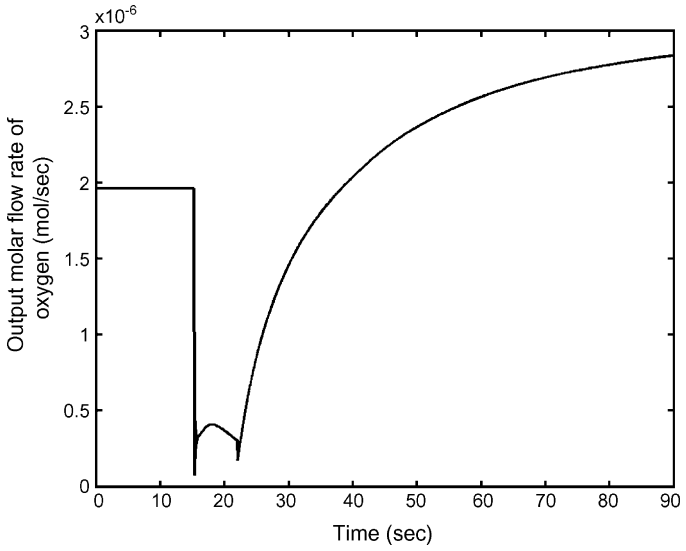

Fig. 28. Output flow rate of oxygen from the PEMFC with ratio control, corresponding to the results shown in Fig. 27.

power density in a relatively short time. Fig. 28 also shows that in the proposed ratio control strategy, the problem of oxygen starvation has been circumvented due to an increase in the input molar flow rate of oxygen.

5. Conclusions

We have studied the transient and input–output responses obtained from a distributed parameter model of the PEMFC, and found that the PEMFC does not exhibit a sign change in the gain of the plant with the inlet molar flow rates of hydrogen and coolant as the manipulated variables. Hence, linear controllers with fixed gain are implemented to satisfy higher power density demand. A ratio control strategy is able to overcome the problem of oxygen starvation; however, the performance of the linear controllers is slow due to the presence of nonlinearities in the dynamic response of the PEMFC. Hence, a nonlinear controller is essential for effective control of the PEMFC over a wide range of power densities. This is the focus of our future work**.** Development of a comprehensive model that includes liquid water transport and flooding is another aspect of future exploration.

Appendix A. Relative gain array matrices for various manipulated variable

The relative gain array is used to predict possible interactive effects between control loops when multiple single input single output (SISO) loops are used. The relative gain (λ_{ij}) between input j and output i is defined as:

$$\lambda_{ij} = \frac{\text{gain between input } j \text{ and output } i \text{ with all other loops are open}}{\text{gain between input } j \text{ and output } i \text{ with all other loops closed}}$$

This gain is based on steady-state gain considerations only; and the gains are obtained from the corresponding dynamic models (Table 2). The extent of interaction between the ith output and the jth input is inferred from the value of relative gain λ_{ij}. A value of λ_{ij} close to 0.5 indicates the presence of strong interaction, and for this case a multi-loop configuration for the control of the multivariable plant is inappropriate. For further details on the RGA analysis, the reader is referred to Seborg et al. [21]. The RGA matrices for various manipulated variables are (refer to Table 2 for nomenclature):

m_1 m_2 1.2055 −0.2055 y_1 −0.2055 1.2055 y_2	m_1 m_3 −0.1344 1.1344 y_1 1.1344 −0.1344 y_2
m_1 m_4 0.8071 0.1928 y_1 0.1928 0.8071 y_2	m_2 m_3 −0.2995 1.2995 y_1 1.2995 −0.2995 y_2
m_2 m_4 0.4299 0.5700 y_1 0.5700 0.4299 y_2	m_2 m_5 1.0005 −5e−4 y_1 −5e−4 1.0005 y_2
m_3 m_4 0.7692 0.2308 y_1 0.2308 0.7692 y_2	m_3 m_5 0.7407 0.2593 y_1 0.2593 0.7407 y_2
m_4 m_5 6.3 −5.3 y_1 −5.3 6.3 y_2	

References

[1] M. Ceraolo, C. Miulli, A. Pozio, J. Power Sources 113 (2003) 131–144.
[2] J.J. Baschuk, L. Xianguo, J. Power Sources 86 (2000) 181–196.
[3] H.H. Voss, D.P. Wilkinson, P.G. Pickup, M.C. Johnson, V. Basura, Electrochem. Acta 40 (3) (1995) 321–328.
[4] T.V. Nguyen, R.E. White, J. Electrochem. Soc. 140 (8) (1993) 2178–2186.
[5] T.F. Fuller, J. Newman, J. Electrochem. Soc. 140 (1993) 1218–1225.
[6] D.M. Bernardi, M.W. Verbrugge, J. Elctrochem. Soc. 139 (9) (1992) 2477–2491.
[7] Z.H. Wang, C.Y. Wang, K.S. Chen, J. Power Sources 94 (2001) 40–50.
[8] M. Wohr, K. Bolwin, W. Schnurnberger, M. Fischer, W. Neubrand, G. Eigenberger, Int. J. Hydrogen Energy 23 (3) (1998) 213–218.
[9] J.C. Amphlett, R.F. Mann, B.A. Peppley, P.R. Roberge, A. Rodrigues, J. Power Sources 61 (1996) 183–188.
[10] P.R. Pathapati, X. Xue, J. Tang, Renewable Energy 30 (2005) 1–22.
[11] Y. Shan, S. Choe, J. Power Sources 145 (2005) 30–39.
[12] J.T. Pukrushpan, A.G. Stefanopolou, H. Peng, Proc. American Control Conference, 2002, pp. 3117–3122.
[13] A. Vahidi, A. Stefanopolou, H. Peng, Proc. American Control Conference, 2004, pp. 834–839.
[14] J. Golbert, D. Lewin, J. Power Sources 135 (2004) 135–151.
[15] J. Golbert, D. Lewin, Proc. IFAC World Congress, 2005.
[16] W. Na, B. Gou, B. Diong, Proc. IEEE Industry Applications Conference, 2005, pp. 2937–2943.
[17] K.C. Lauzze, D.J. Chmielewski, Ind. Eng. Chem. Res. 45 (2006) 4661–4670.
[18] S. Yerramalla, A. Davari, A. Feliachi, Proc. IEEE Power Engg. Society Summer Mtg, 2002, pp. 82–86.
[19] J.S. Yi, T.V. Nguyen, J. Electrochem. Soc. 145 (1998) 1149–1159.
[20] T.E. Springer, T.A. Zawodzinski, S. Gottesfeld, J. Electrochem. Soc. 138 (1991) 2334–2342.
[21] D.E. Seborg, T.F. Edgar, D.A. Mellichamp, Process Dynamics and Control, Wiley, New York, 1989.